CHEMISTRY
A EUROPEAN JOURNAL

DOI: 10.1002/chem.200800827

Ruthenium(II) Pyridylamine Complexes with Diimine Ligands Showing Reversible Photochemical and Thermal Structural Change

Takahiko Kojima,*[a] Tsuyoshi Morimoto,[a] Taisuke Sakamoto,[b] Soushi Miyazaki,[a] and Shunichi Fukuzumi*[a]

Abstract: Ruthenium(II)–TPA–diimine complexes, $[Ru(TPA)(diimine)]^{2+}$ (TPA = tris(2-pyridylmethyl)amine; diimine = 2,2′-bipyridine (bpy), 2,2′-bipyrimidine (bpm), 1,10-phenanthroline (phen)) were synthesized and characterized by spectroscopic and crystallographic methods. Their crystal structures demonstrate severe steric hindrance between the TPA and diimine ligands. They exhibit drastic structural changes on heating and photoirradiation at their MLCT bands, which involve partial dissociation of the tetradentate TPA ligand to exhibit a facially tridentate mode accompanied by structural change and solvent coordination to give $[Ru(TPA)(diimine)(solvent)]^{2+}$ (solvent = acetonitrile, pyridine). The incoming solvent molecules are required to have π-acceptor character, since σ-donating solvent molecules do not coordinate. The thermal process is irreversible dissociation to give the solvent-bound complexes, which takes place by an interchange associative mechanism with large negative activation entropies. The photochemical process is a reversible reaction reaching a photostationary state, probably by a dissociative mechanism involving a five-coordinate intermediate to afford the same product as obtained in the thermal reaction. Quantum yields of the forward reactions to give dissociated products were lower than those of the backward reactions to recover the starting complexes. In the photochemical process, the conversions of the forward and backward reactions depend on the absorption coefficients of the starting materials and those of the products at certain wavelength, as well as the quantum yields of those reactions. The reversibility of the motions can be regulated by heating and by photoirradiation at certain wavelength for the recovery process. In the bpm system, we could achieve about 90% recovery in thermal/photochemical structural interconversion.

Keywords: ligand effects · N ligands · photochromism · reaction mechanisms · ruthenium

Introduction

Controlling molecular motions has been intensively investigated with regard to the development of molecular devices to perform precise functions at the molecular level.[1] Molecular motions play indispensable roles not only in biological systems to achieve enzymatic functionality but also in artificial functional materials. In biological systems, as represented by ATP synthase producing ATP (adenosine triphosphate) as an energy source of life,[2] the F1 unit of ATP synthase rotates in one direction due to a concentration gradient of protons between the inside and outside of the membrane in the course of ATP synthesis.[3] On the other hand, photoisomerization of retinal in rhodopsin is responsible for the conversion of light to neuronal signaling for visualization.[4]

Chemical design and synthesis allow access to functional molecules offering great diversity, better structural and dynamic control, as well as feasibility of observation and analysis. Artificial molecular devices have been developed by using mainly organic components which exhibit reversible structural changes driven by external stimuli including light,[5] heat and light,[6] pH control (acid/base control),[7]

[a] Prof. Dr. T. Kojima, T. Morimoto, Dr. S. Miyazaki, Prof. Dr. S. Fukuzumi
Department of Material and Life Science
Graduate School of Engineering
Osaka University and SORST (JST)
2-1 Yamada-oka, Suita, Osaka 565-0871 (Japan)
Fax: (+81) 6-6879-7370
E-mail: kojima@chem.eng.osaka-u.ac.jp
fukuzumi@chem.eng.osaka-u.ac.jp

[b] T. Sakamoto
Department of Chemistry
Graduate School of Science
Kyushu University
6-10-1 Hakozaki, Higashi-ku, Fukuoka 812-8581 (Japan)

Supporting information for this article is available on the WWW under http://dx.doi.org/10.1002/chem.200800827.

WILEY InterScience DISCOVER SOMETHING GREAT
© 2008 Wiley-VCH Verlag GmbH & Co. KGaA, Weinheim

redox control,[8] and metal complexation.[9] Among these compounds, diaryl ethene[10] and fulgide[11] derivatives have been shown to exhibit photochromic behavior in which the photochemical products can be isolated and characterized.

Transition-metal complexes have also been recognized as useful platforms for the construction of molecular devices showing mechanical motions. Owing to their wide range of geometrical and electronic structures, abundant functionality can be expected for molecular devices based on metal complexes. So far, structural changes of ligands in the coordination spheres of metal complexes have been achieved by using redox reactions[12] and photoirradiation.[13] Redox-switchable reversible structural change of metal complexes has been reported by using a Cu^{II}/Cu^{I} redox couple to induce geometrical change in the course of the process by Canary and co-workers,[14] and a strategy using ferrocene-containing hemilabile ligands by Mirkin and co-workers.[15] Photochemical structural change has also been investigated in metal complexes, especially ruthenium complexes.[16] Meyer and co-workers described reversible *cis–trans* photoisomerization of Ru^{II} diimine complexes,[17] and Sauvage and co-workers used a ruthenium complex to construct a catenane that can change its structure reversibly by photochemical ligand dissociation on addition of tetraethylammonium chloride and thermal ligand substitution.[18] However, no example has been reported for reversible structural change accompanying acceptance and release of external molecules based on different driving forces to distinguish the direction of motion. To control the motion, perfect discrimination of inputs as driving forces and bistability of the molecules should be designed.

Here we describe the synthesis and characterization of Ru^{II} complexes bearing tris(2-pyridylmethyl)amine (TPA) and the diimine ligands 2,2′-bipyridine (bpy),[19] 2,2′-bipyrimidine (bpm), and 1,10-phenanthroline (phen) and their drastic structural changes in response to external stimuli including photoirradiation and heating. In this structural change, the TPA ligand exhibits reversible dissociation and binding, whereby its coordination varies between the normal tetradentate mode and a facial tridentate mode in association with selective binding and release of π-acceptor molecules.

Results and Discussion

Preparation of Ru–TPA–diimine complexes: Reactions of bis-μ-chloro dinuclear complexes $[Ru_2Cl_2(L)_2](ClO_4)_2$ (L = TPA, 5-Me-TPA, 5-Me_3-TPA)[20] with the diimines 2,2′-bipyridine (bpy), 2,2′-bipyrimidine (bpm), and 1,10-phenanthroline (phen) in MeOH at reflux under N_2 gave $[Ru(L)(diimine)]X_2$ in good to moderate yields. After cooling to room temperature, NH_4PF_6 was added to precipitate the PF_6^- salts of these complexes. Structural formulas of representative complexes **1–3** are shown in Scheme 1.

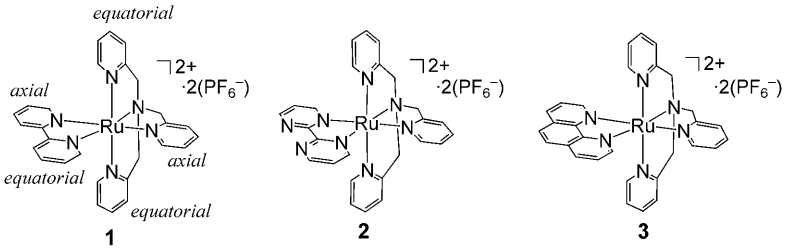

Scheme 1. Schematic description of complexes **1–3** with the definition of the positions in the complexes used throughout this work.

Crystal structures of Ru–TPA–diimine complexes: The molecular structures of complexes **1–3** were determined by X-ray crystallography; ORTEP drawings of their cationic moieties are depicted in Figure 1. Selected bond lengths and angles are listed in Table 1. These complexes exhibit slightly distorted octahedral geometries consisting of the tetradentate TPA ligand and bidentate diimine ligands. The bond lengths around the Ru^{II} centers fall in the normal range of Ru^{II}–N bonds,[21] but Ru1–N2 and Ru1–N6 are slightly longer than the other Ru–N bonds.

A characteristic feature of the structures is the tilt of the axial pyridine ring of TPA in the coordination spheres, due to steric hindrance between the axial pyridine moiety and the aromatic ring of the diimine ligand, which binds to the equatorial plane of the complexes (see Scheme 1). The C6···C19 distances are 3.29, 3.33, and 3.37 Å in **1–3**, respectively. The dihedral angles between the axial pyridine ring and the equatorial aromatic ring of the diimine ligands and intraligand dihedral angles of the diimine ligands are summarized in Table 2. The dihedral angles between the axial pyridine ring of the TPA ligand and the equatorial pyridine moiety of the diimine ligands are fairly large (42.8° in **1**, 33.8° in **2**, and 40.3° in **3**) and the N2-Ru1-N5 bond angles, which are all larger than 100°, reflect the severe steric hindrance between them. In addition, this tilt eventually causes chirality around the metal center to give racemic mixtures of right- and left-tilted enantiomers in the monoclinic and triclinic space groups in the solid state.

Spectroscopic characterization of Ru–TPA–diimine complexes: Absorption spectra of **1–3** in CH_3CN (Figure 2) exhibit metal-to-ligand charge transfer (MLCT) bands at 453 (2.737 eV), 480 (2.583 eV), and 423 nm (2.931 eV). These MLCT absorptions are similar to those of $[Ru(bpy)_3]^{2+}$ (452 nm),[22] $[Ru(bpm)_3]^{2+}$ (454 nm),[22] and $[Ru(phen)_3]^{2+}$ (422 and 447 nm),[23] respectively.

In the ^1H NMR spectra of **1–3**, one singlet and one AB quartet due to the methylene protons of the axial pyridyl-

 © 2008 Wiley-VCH Verlag GmbH & Co. KGaA, Weinheim

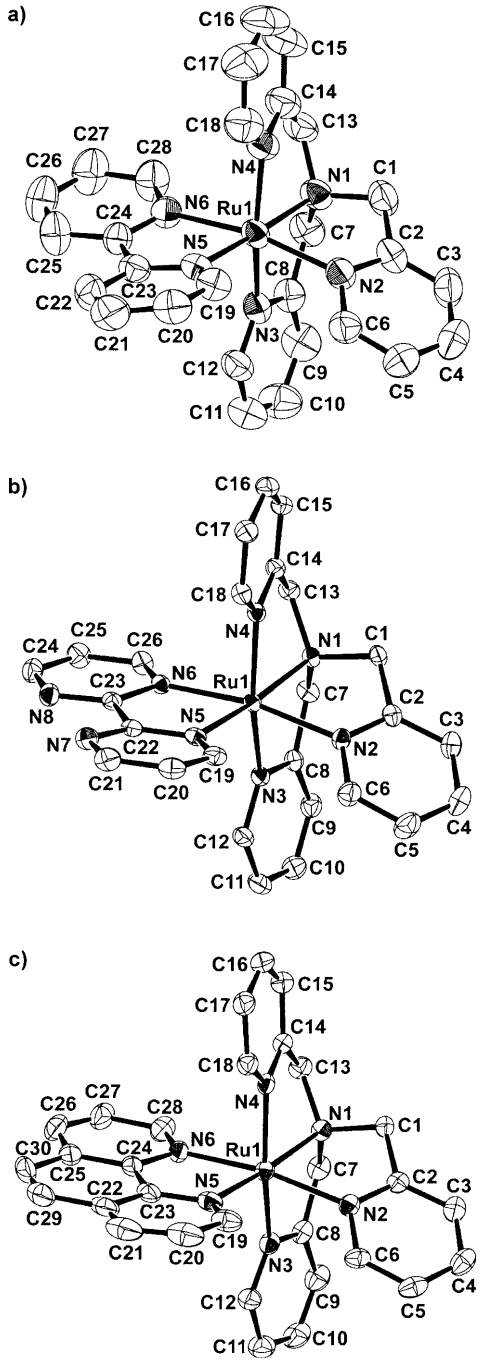

Figure 1. Crystal structures of the cationic moieties of **1** (a), **2** (b), and **3** (c) with atomic numbering schemes for non-hydrogen atoms. Hydrogen atoms are omitted for clarity. Each atom is described with thermal ellipsoids at 50% probability.

methyl arm and those of the two equatorial pyridylmethyl groups, respectively, were observed, in accordance with the σ_h symmetry of the complexes in solutions.[20] This indicates that the tilt of the axial pyridine ring observed in the crystal structures is dynamically averaged on the NMR timescale. As a representative example, the ^{1}H NMR spectrum of **1** is shown in Figure 3a. Peak assignments were made by peak integration and ^{1}H,^{1}H COSY (see Experimental Section).

Table 1. Selected bond lengths [Å] and angles [°] of **1**, **2**, and **3**.

	1[a]	**2**	**3**
Ru1−N1	2.085(3)	2.093(3)	2.084(2)
Ru1−N2	2.102(3)	2.101(3)	2.115(2)
Ru1−N3	2.048(3)	2.068(3)	2.042(3)
Ru1−N4	2.078(3)	2.091(3)	2.079(2)
Ru1−N5	2.065(3)	2.086(3)	2.074(3)
Ru1−N6	2.101(2)	2.092(2)	2.096(2)
N1-Ru1-N2	79.1(1)	79.9(1)	79.0(1)
N1-Ru1-N3	83.5(1)	82.6(1)	84.5(1)
N1-Ru1-N4	80.6(1)	79.8(1)	80.0(1)
N5-Ru1-N6	77.3(1)	77.8(1)	79.1(1)
N1-Ru1-N5	175.9(1)	171.7(1)	172.8(1)
N2-Ru1-N6	167.9(1)	168.8(2)	169.5(1)
N2-Ru1-N5	100.6(1)	100.4(1)	100.9(1)

[a] See ref. [19].

Table 2. Selected dihedral angles [°] for the axial (ax) pyridine ring of TPA and equatorial (eq) pyridine moiety of the diimines and those in the diimine ligands.[a]

	1	**2**	**3**	**7**	**8**
ax pyridine/eq pyridine	42.8	33.8	40.3		
diimine	13.5	5.1	3.1	4.6	1.7

[a] Estimated by using Mercury program.

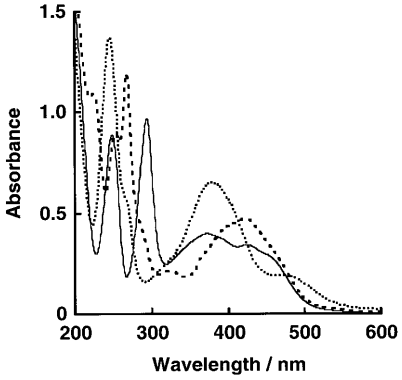

Figure 2. Absorption spectra of **1** (solid line), **2** (dotted line), and **3** (dashed line) in CH_3CN.

The singlets due to the methylene protons of the axial pyridylmethyl arm were observed at $\delta = 4.66$, 4.70, and 4.74 ppm for **1**–**3**, respectively. The AB quartet with large geminal coupling of methylene protons of the equatorial pyridylmethyl arms is observed at $\delta = 5.07$ and 5.43 ppm for **1**, $\delta = 5.11$ and 5.35 ppm for **2**, and $\delta = 5.16$ and 5.57 ppm for **3**, respectively (Supporting Information, Figures S2 and S3). The lowest chemical shifts were observed for the CH groups next to the coordinated nitrogen atom of the equatorial heteroaromatics in the diimine ligands.

Thermal structural change: Complexes **1**–**3** exhibit drastic and complete structural change in the course of heating in CH_3CN. The reactions were followed by ^{1}H NMR and absorption spectroscopy.

 © 2008 Wiley-VCH Verlag GmbH & Co. KGaA, Weinheim

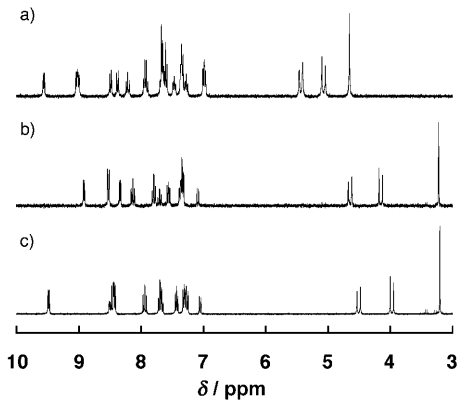

Figure 3. ^{1}H NMR spectra of **1** (a), **4** (b), and **7** (c) in CD_3CN.

In the course of heating **1** in CD_3CN, the singlet assigned to the axial methylene protons at $\delta = 4.66$ ppm in the ^{1}H NMR spectrum diminished and a new upfield-shifted singlet emerged at $\delta = 3.22$ ppm (Figure 3b). The AB quartet at $\delta = 5.07$ and 5.43 ppm also shifted, to $\delta = 4.65$ and 4.16 ppm. The ^{1}H,^{1}H COSY spectrum of the thermal product allowed us to make complete assignments for the signals in the aromatic region. The peaks due to the protons of the bpy ligand showed only one set of 2-substituted pyridine rings, that is the bpy ligand is coordinated to the Ru^{II} center in a symmetric mode, in sharp contrast to that in **1**, in which the asymmetrically bound bpy ligand show two sets of 2-substituted pyridine rings. This suggests that the thermal product has a different geometry from **1** but is still σ_h-symmetric. In addition, the reaction product in CH_3CN exhibited a singlet assignable to the methyl protons of coordinated CH_3CN at $\delta = 2.27$ ppm, which is shifted slightly downfield relative to free CH_3CN and indicates N-bound CH_3CN.[24] The ESIMS spectrum of the product exhibited a peak cluster with an isotopic pattern at m/z 734.2. This corresponds to $\{[Ru(TPA)(bpy)(CH_3CN)](PF_6)\}^+$ ($[M-PF_6^-]^+$), and its simulated isotopic pattern is consistent with the observed one. These observations suggest that the thermal product may have an uncoordinated pyridylmethyl arm and one molecule of coordinated acetonitrile with a symmetric plane across the center of the bpy ligand, as shown in Scheme 2.

Coordination of a solvent molecule also proceeded in pyridine at a similar rate (1.54×10^{-7} s^{-1} at 20 °C) to give pyridine complex $[Ru(TPA)(bpy)(pyridine)]^{2+}$, which was confirmed by ESIMS observation of a peak cluster at m/z 777.0 with a isotopic pattern corresponding to $\{[Ru(TPA)(bpy)(C_5D_5N)](PF_6)\}^+$, generated in $[D_5]$pyridine.[19] However, the reaction does not occur in σ-donating solvents such as H_2O and MeOH or noncoordinating solvents such as dichloromethane. In DMSO, which should act as a strong σ-donor in O-bound form but a strong π-acceptor in S-bound form, no reaction was observed up to 100 °C. Thus, the incoming ligand should have π-acceptor character and low hindrance to attack the Ru^{II} center (vide infra).

We could not obtain the crystal structure of the dissociated thermal product **4**, but we could trap it by reaction with an excess (50 equiv) of $Et_4N^+Cl^-$ in CH_3CN (Scheme 2). The isolated product was stable and exhibited the same NMR pattern as observed for the thermal dissociation product (Figure 3c), which reflects conservation of the configuration in the course of ligand exchange from acetonitrile to chloride. The ESIMS spectrum of the chlorinated product exhibited a peak cluster at m/z 583.3 with a specific isotopic pattern consistent with $[RuCl(TPA)(bpy)]^+$ $[M^+]$.

Recrystallization of the crude chlorinated product from acetone afforded a single crystal suitable for determining the crystal structure of $[RuCl(TPA)(bpy)]PF_6$ (**7**), as shown in Figure 4a. Selected bond lengths and angles are summarized in Table 3. The crystal structure clearly demonstrates a drastic structural change in the dissociated product. One of the pyridylmethyl arms has dissociated from the Ru^{II} center and is uncoordinated. Thus, the geometry of complex **7** is totally different from that of **1** and is composed of a symmetrically bound bidentate bpy ligand and a facially tridentate TPA ligand.[25,26] The dihedral angle between the two pyridine rings of the bpy ligand in **7** is 4.6° (Table 2), which is less than half of that observed in **1**, that is, the steric tension of the ligand is relaxed in the dissociation product. In addition, the Ru1–N1 bond length (the tertiary amino group) is longer (2.125(6) Å) than those found in **1**, probably due to the strong interaction of Cl^- with the Ru^{II} center at the *trans* position exerting a *trans* influence. The fact that N3-Ru1-N4 bond angle (85.3 (2)°) is smaller than 90° suggests that steric effects of the 6- and 6′-CH groups push the pyridine rings away from them.

For complexes, **2** and **3**, we also observed thermal dissociation to give products with facially tridentate TPA ligands and symmetrically coordinated diimine ligands. In the ^{1}H NMR spectra of **2** and **3**, we observed upfield-shifted singlets and AB quartets for the methylene protons of the uncoordinated and equatorial pyridylmethyl arms, respectively, and resonances in

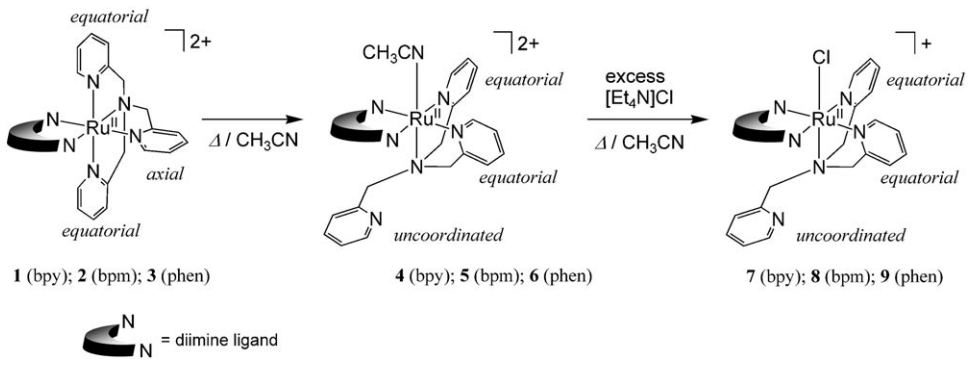

Scheme 2. Thermal reactions of **1**–**3** in acetonitrile.

 © 2008 Wiley-VCH Verlag GmbH & Co. KGaA, Weinheim

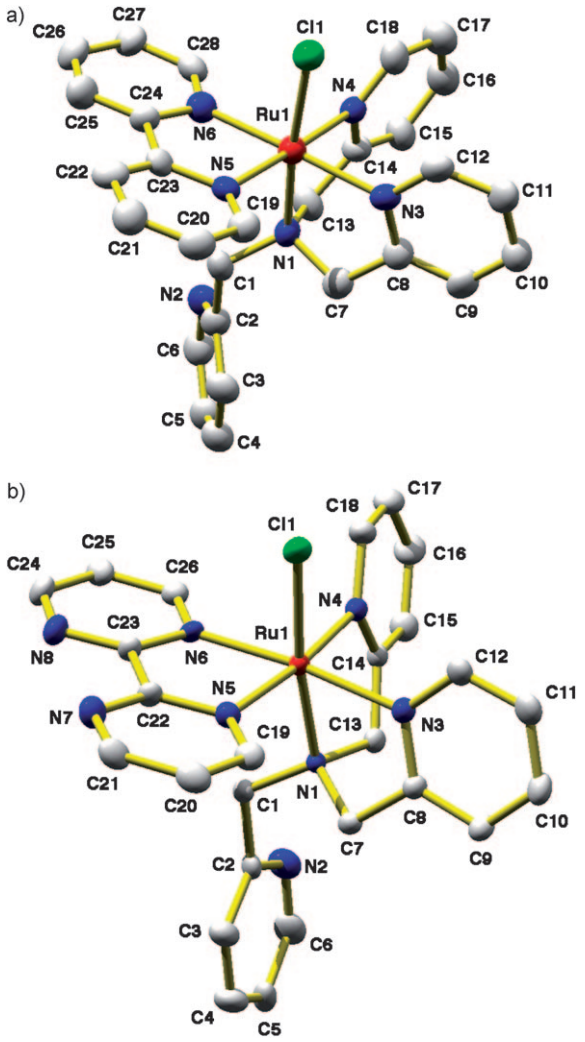

Figure 4. Crystal structures of the cationic moieties of **7** (a) and **8** (b) with 50% probability thermal ellipsoids (POV-RAY program). Hydrogen atoms are omitted for clarity.

Table 3. Selected bond lengths [Å] and angles [°] of **7** and **8**.

	7	**8**
Ru1–Cl1	2.419(2)	2.4010(6)
Ru1–N1	2.125(6)	2.143(2)
Ru1–N3	2.058(8)	2.064(2)
Ru1–N4	2.051(7)	2.072(2)
Ru1–N5	2.049(8)	2.045(2)
Ru1–N6	2.042(9)	2.043(2)
N1-Ru1-N3	81.3(2)	81.74(8)
N1-Ru1-N4	81.2(2)	79.21(8)
N5-Ru1-N6	78.9(2)	79.38(8)
N3-Ru1-N4	85.3(2)	90.49(7)

the aromatic region exhibited symmetric patterns for the protons of the bpm and phen ligands, respectively. Singlets due to the acetonitrile ligands in the products derived from dissociation of **2** and **3** were observed at $\delta = 2.27$ ppm in both bases as well as in **1**; ESIMS spectra of those products showed peak clusters corresponding to {[Ru(TPA)(bpm)-$(CH_3CN)](PF_6)\}^+$ ($[M^{2+}+PF_6^-]^+$) at *m*/*z* 736.2 and {[Ru-(TPA)(phen)$(CH_3CN)](PF_6)\}^+$ ($[M^{2+}+PF_6^-]^+$) at *m*/*z* 758.2, and simulated isotopic patterns completely matched the observed spectra. In addition, complexes **5** and **6** also underwent substitution of the CH_3CN ligands by Cl^- in reactions with an excess of Et_4NCl to form corresponding chlorido complexes **8** and **9** (Scheme 2), which were confirmed by ESIMS, absorption and NMR spectroscopy, and elemental analysis.

We obtained a single crystal of **8** by recrystallization from acetone/hexane layered solution. The crystal structure of $[RuCl(TPA)(bpm)]PF_6$ (**8**) as shown in Figure 4b. Selected bond lengths and angles are listed in Table 3. The geometry of the complex is almost identical to that of **7**, but has a longer Ru1–N1 bond (2.143(4) Å) and a larger N2-Ru1-N3 bond angle (92.5(1)°) than **7**. The dihedral angle between the two pyrimidine rings in the bpm ligand of 1.7° is less than half that in **2**, as is also the case for **7** (Table 2).

The chloro complexes exhibited absorption maxima at 503 nm for **7**, 539 nm for **8**, and 495 nm for **9**, which were assigned to MLCT bands from the Ru^{II} center to the diimine ligands.[27] The redshift could be due to interaction of 3p electrons of Cl^- with dπ electrons of the Ru^{II} center, which elevates the energy level of the dπ orbital and results in smaller energy gaps between the dπ orbital and the π* orbitals of diimine ligands.

Elucidating the thermal dissociation process: The question arises which pyridine moiety is released from the metal center in acetonitrile in the structural changes in the coordination sphere of the $[Ru(TPA)(diimine)]^{2+}$ complexes accompanying solvent coordination on thermal dissociation. The structural change was elucidated by introduction of one methyl group at the 5-position of one of pyridine rings of TPA.

First, we prepared the 5-Me_3-TPA analogue of **1**, [Ru(5-Me_3TPA)(bpy)]$(PF_6)_2$ (**10**). This complex also exhibited thermal structural change in acetonitrile, and the reaction was followed by ^1H NMR spectroscopy (Figure S4 in the Supporting Information). In the ^1H NMR spectrum of **10** in CD_3CN, a singlet due to the methyl group attached to the axial pyridine ring was observed at $\delta = 2.28$ ppm and a singlet assigned to the methyl groups attached to the equatorial pyridine ring was observed at $\delta = 1.97$ ppm with 1:2 integration ratio of peak intensity. The sample was heated for 8 h and the NMR spectrum measured again. The final product, $[Ru(5\text{-}Me_3TPA)(bpy)(CD_3CN)]^{2+}$ (**11**), exhibited two singlets at $\delta = 2.29$ and 2.36 ppm with peak intensity ratio of 1:2. We assigned the former to the methyl group attached to the uncoordinated pyridine ring and the latter to the two equatorial pyridine rings.

Next we applied 5-Me-TPA as ligand to track the methyl-substituted pyridine ring in the course of the thermal structural change by ^1H NMR spectroscopy (Figure S5 in the Supporting Information). We synthesized [Ru(5-Me-TPA)-(bpy)]$(PF_6)_2$ (**12**) as a 2:1 mixture of two isomers in which the methyl-substituted pyridine moiety binds to one of the

 © 2008 Wiley-VCH Verlag GmbH & Co. KGaA, Weinheim

two equatorial positions (**12**-equatorial) and the axial position (**12**-axial), as shown in Scheme 3.

In the NMR spectrum of the mixture of **12**-axial and **12**-equatorial, the singlet assigned to the methyl group of **12**-axial was observed at $\delta = 2.27$ ppm, and that of **12**-equatorial at 1.97 ppm, with a peak intensity ratio of 1:2. Heating the NMR sample containing **12**-axial and **12**-equatorial resulted in new singlets at $\delta = 2.29$ and 2.35 ppm with a peak intensity ratio of 1:2. We assigned these signals to the methyl group of the uncoordinated pyridine ring (**13**-uncoordinated) and the coordinated pyridine ring in one of the two equatorial positions (**13**-equatorial), respectively, as shown in Scheme 3, on the basis of the data obtained for $[Ru(5\text{-}Me_3TPA)(bpy)(CD_3CN)]^{2+}$ derived from **10**. This indicates that dissociation of the pyridine moiety occurs at the axial position.

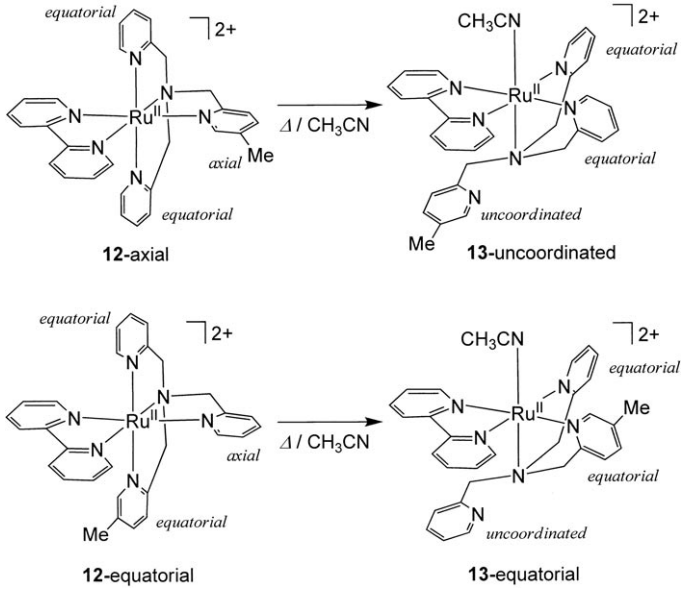

Scheme 3. Thermal dissociation of **12**.

Kinetics and thermodynamics of thermal structural change: To shed light on the details of the thermal structural change of **1**–**3**, we measured first-order rate constants in CH_3CN at various temperatures (Table 4).

Table 4. First-order rate constants k [s^{-1}, $\times 10^5$] and activation parameters for the thermal structural change of **1**–**3** in CD_3CN

T	**1**	**2**	**3**
323 K	0.87	0.47	0.43
k(328 K)	1.40	0.70	0.65
k(333 K)	2.27	1.26	1.06
k(338 K)	4.04	2.07	1.88
k(343 K)	5.27	2.85	2.46
$\Delta H^{\neq}$ [kJ mol^{-1}]	83 ± 5	82 ± 4	82 ± 5
$\Delta S^{\neq}$ [J mol^{-1} K^{-1}]	−85 ± 13	−93 ± 12	−94 ± 14

The thermal structural change of each complex obeyed first- order kinetics in the range of 323–343 K in CH_3CN. The temperature dependence of the first-order rate constants afforded linear Eyring plots for the three complexes (Figure S1, Supporting Information). The activation enthalpies $\Delta H^{\neq}$ and activation entropies $\Delta S^{\neq}$ of the reactions were also determined (Table 4). These values are similar to those observed in thermal isomerization of Ru^{II} alloxazine complexes by coordination of CH_3CN ($\Delta H^{\neq} = 92$ kJ mol^{-1} and $\Delta S^{\neq} = -38$ J mol^{-1} K^{-1}).[28] In the case of intramolecular rearrangement of an Ru^{II} TPA β-diketonato complex without bond rupture, the activation parameters are totally different ($\Delta H^{\neq} = 50$ kJ mol^{-1} and $\Delta S^{\neq} = -213$ J mol^{-1} K^{-1}).[29] Changing the counteranion from PF_6^- to ClO_4^- did not have any influence on the activation parameters. All complexes showed similar activation parameters which indicate that the reaction proceeds by the same reaction mechanism for **1**–**3**. The large negative activation entropies suggest that the reaction proceeds by an interchange associative (I_a) mechanism involving interaction of the acetonitrile molecule with the Ru^{II} center to displace the axial pyridine ring of the TPA ligand.[30] This is consistent with the above observation that in DMSO formation of the thermal dissociation product with the S-bound form of the solvent as a π acceptor does not occur due to its bulkiness. The lack of formation of the DMSO complex is probably due to steric hindrance in the associative transition state. The positive activation enthalpies suggest compensation of dissociation of the strongly bound pyridine moiety and weaker solvent coordination in the transition state.

Photochemical reversible structural change: Photoirradiation of solutions of **1**–**3** in acetonitrile was examined by monochromated light with a fluorescence spectrophotometer at room temperature. The complexes exhibited photochemical structural change on irradiation at MLCT bands that allowed us to observe spectral change in their absorption and NMR spectra. In the course of the photochemical structural change of **1**–**3**, their NMR spectra showed the same, albeit incomplete, spectral change that was observed in the thermal reactions. The photochemical reactions result in mixtures of starting complexes **1**–**3** and products **4**–**6**, respectively, as photostationary states. In contrast to the irreversible thermal process to give the dissociation products, the photochemical reaction is reversible.

In the course of the photoirradiation, we observed UV/Vis spectral change (Figure 5). The spectral change was not complete, in contrast to that in thermal reactions, and this is consistent with NMR observations. The incompleteness of the reaction should stem from the fact that the starting complexes and the products have the same Ru^{II} diimine moieties as chromophores. As can be seen in the absorption spectra, photoexcitation at the MLCT bands results in excitation of both species. However, since we can isolate the photochemical dissociation products as the thermal reaction products in pure form, we can determine the quantum yields of both the forward and backward reactions separately.

 © 2008 Wiley-VCH Verlag GmbH & Co. KGaA, Weinheim

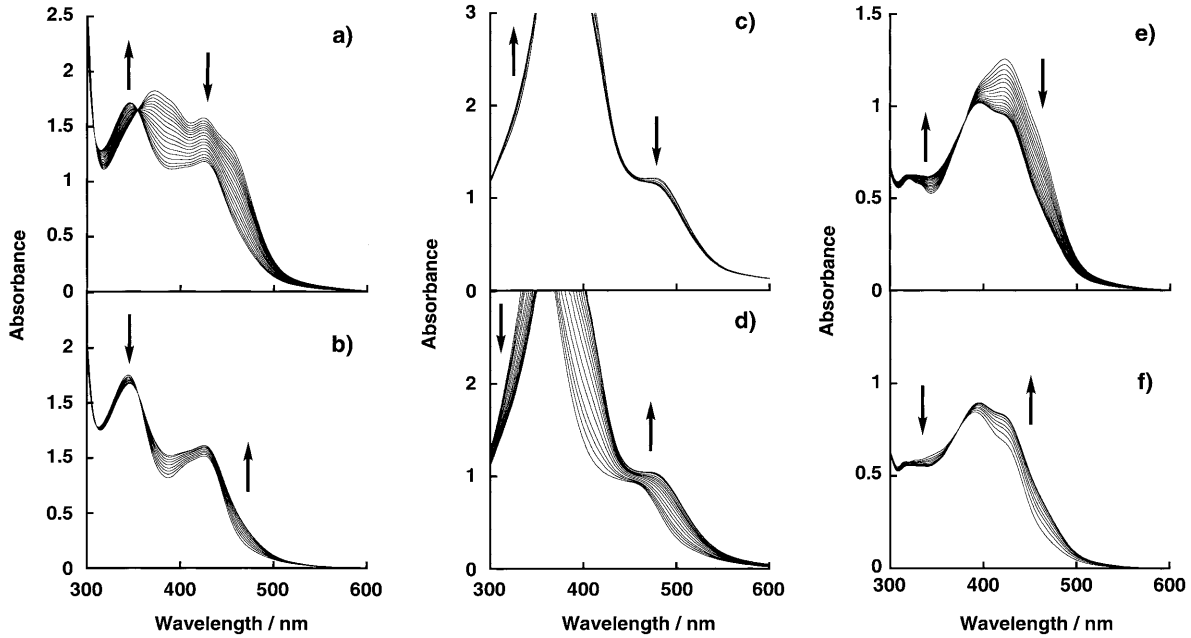

Figure 5. Absorption spectral change in the photochemical structural changes of **1** (a), **4** (b), and **2** (c) and of **5** (d), **3** (e), and **6** (f) in CH_3CN at room temperature.

The photochemical conversion of starting complexes **1–3** to the photostationary states consisting of these complexes and photoproducts **4–6** was monitored by absorption spectroscopy. The course of the concentration of each component with time in the forward and backward reactions for the three diimine systems are summarized in Figure 6. The concentrations of the two components converge to the same value from both sides.

Quantum yields of the photochemical reversible structural change of **1–3** in CH_3CN were determined for both forward and backward reactions by using $[Fe(oxalato)_3]^{3-}$ as an actinometer at room temperature with monochromated photoirradiation at 423 nm. The quantum yields and conversions of the backward reactions are summarized in Table 5.

For bpy complexes **1** and **4**, the quantum yields of **1**→**4** and and **4**→**1** are 0.0021 and 0.0057; for bpm complexes **2** and **5**, the quantum yields of **2**→**5** and **5**→**2** are 0.0017 and 0.028; and for phen complexes **3** and **6**, the quantum yields of **3**→**6** and **6**→**3** are 0.0027 and 0.011, respectively. In all cases, the quantum yields of the backward reactions (Φ_b) are higher than those of the forward reactions (Φ_f). The conversions of the backward reactions are related to quantum yields by Equation (1),[31] in which ε_{coord} stands for the absorption coefficient of the original complex (**1–3**) with the absorption coefficients. Based on Equation (1), we calculated the conversions of the backward reaction for the three systems as listed in Table 5.

$$\text{Conversion}_{\text{uncoord}\rightarrow\text{coord}} = \frac{\Phi_b \varepsilon_{\text{uncoord}}}{\Phi_b \varepsilon_{\text{uncoord}} + \Phi_f \varepsilon_{\text{coord}}} \quad (1)$$

The calculated conversions are fairly consistent with those observed in the NMR measurements. Complex **5** exhibited the highest conversion of 89% for the backward reaction to form **2**. This indicates that the thermal and photochemical interconversion between **2** and **5** can be achieved to 89% for the **2**→**5**→**2** pathway, accompanying the drastic structural change involving acceptance and release of external molecules with π-acceptor character.

Together with the results of both thermal and photochemical reactions, we propose the reversible interconversion of the Ru TPA diimine complexes in CH_3CN shown in Scheme 4, which describes that of complexes **2** and **5** as a representative example. In the one-way thermal structural change, the nucleophilic attack of a less bulky solvent molecule at the Ru^{II} center occurs to form an associative transition state and displace the axial pyridine moiety of the tetradentate TPA ligand. The transition state would be followed by structural change to give the dissociation product with facially tridentate TPA ligand and a solvent molecule such as CH_3CN or pyridine.

The photochemical process is started by photoexcitation of the complexes to form triplet MLCT excited states ^{3}(MLCT)*, which can be converted to metal-centered triplet states ^{3}(MC)*.[32] The ^{3}(MC)* states are d–d transition states of the complexes, and one of the d_π electrons is located in d_σ orbitals to facilitate thermal ligand dissociation due to the electric repulsion between the photoexcited electron in the d_σ orbital and σ-donated lone pair of the pyridine moiety to form five-coordinate transition states in a dissociative (D) mechanism.[30,33] This five-coordinate transition state undergoes solvent coordination concomitant with the structural change. This proposal is also supported by DMSO coordination in photochemical process to give two kinds of photoproducts $[Ru(TPA)(bpy)(DMSO)]^{2+}$,[34] in sharp contrast to the lack of observation of thermal structural change in

 © 2008 Wiley-VCH Verlag GmbH & Co. KGaA, Weinheim

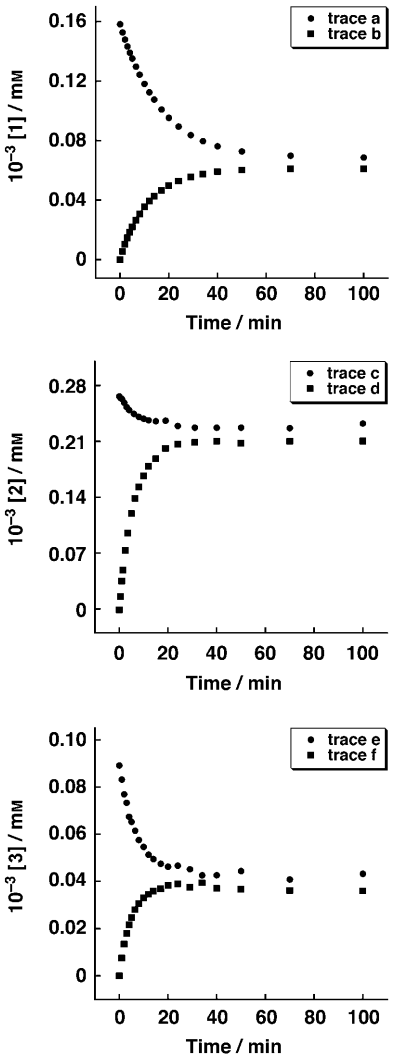

Figure 6. Time course of the concentrations of the starting complexes and the photoproducts in CH_3CN. a) **1**→**1**+**4**. b) **4**→**1**+**4**. c) **2**→**2**+**5**. d) **5**→**2**+**5**. e) **3**→**3**+**6**. f) **6**→**3**+**6**. Photoirradiation was performed at 423 nm for the bpy complexes (**1** and **4**), 453 nm for the bpm complexes (**2** and **5**), and 423 nm for the phen complexes (**3** and **6**).

Table 5. Quantum yields and conversions of structural change and recovery.

Diimine ligand	Φ_f (coord→ uncoord+ coord)[a]	Φ_b (uncoord→ coord+ uncoord)[a]	Wavelength [nm]	Calcd conversion (uncoord→ coord+ uncoord)[b]	Obsd conversion (uncoord→ coord+ uncoord)[c]
bpy	0.0021	0.0057	423	63	40
			453	50	35
			480	40	20
bpm	0.0017	0.028	423	89	78
			453	92	89
			480	91	85
phen	0.0027	0.011	423	70	65
			453	57	56
			480	48	45

[a] Determined at 423 nm. [b] Calculated on the basis of Equation (1). [c] Determined by peak integration of ^1H NMR signals.

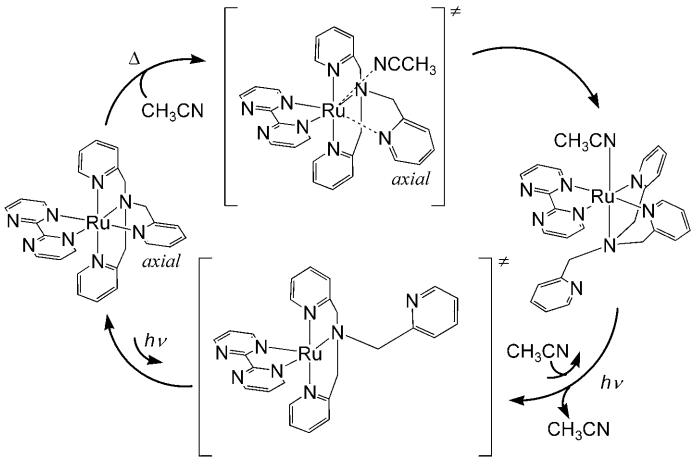

Scheme 4. Proposed reaction mechanism of thermal and photochemical interconversion between **2** and **5** in CH_3CN.

DMSO up to 100 °C: The bulky DMSO molecule can coordinate to the five-coordinate Ru^{II} center without any steric hindrance.

Chloro complex **7** also exhibited photochemical reaction in CH_3CN at room temperature on photoirradiation at 580 nm, where apparently no absorption was observed for **1** and **4**. The reaction was followed by absorption spectroscopy, and we observed initially an increase of the absorption at 453 nm due to **1** over 30 min, as shown in Figure 7a, with

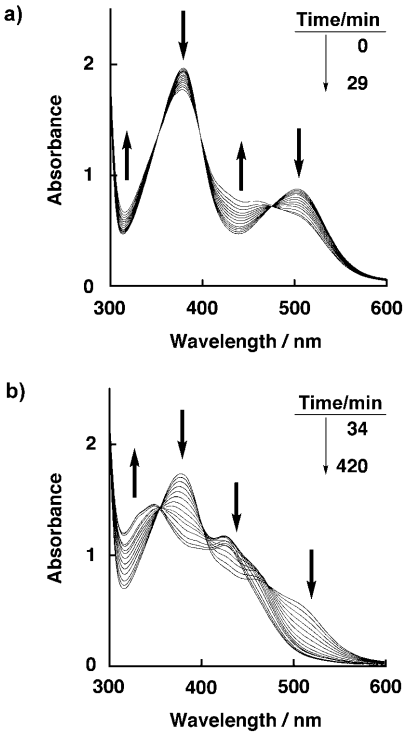

Figure 7. Absorption spectral change of **7** in the course of photoirradiation at 580 nm in CH_3CN at room temperature. a) 0–29 min. b) 34–420 min.

 © 2008 Wiley-VCH Verlag GmbH & Co. KGaA, Weinheim

isosbestic points at 476, 396, and 352 nm. Further reaction was observed to give a mixture of **1** and acetonitrile complex **4** on prolonged photoirradiation (Figure 7) with an isosbestic point at 352 nm, and slight amount of **7** could also be observed in the ESIMS spectrum of the mixture. This result clearly indicates that the photoproduct is pyridine-coordinated product **1**, rather than the dissociated complex **4** (Scheme 5). Thus, photodissociation of Cl^- is followed by intramolecular pyridine coordination to recover the staring complex, rather than intermolecular CH_3CN coordination.

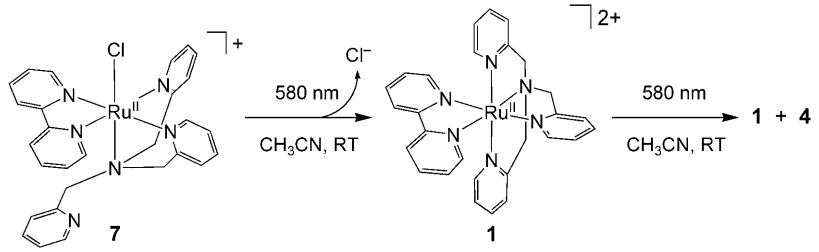

Scheme 5. Photoreaction of **7** in the course of photoirradiation at 580 nm in CH_3CN.

Conclusion

We have described the synthesis and characterization of Ru^{II}–TPA–diimine complexes which exhibit photochromic behavior involving clear and dramatic structural change. Thermal reaction of $[Ru(TPA)(diimine)]^{2+}$ with thr tetradentate TPA ligand affords $[Ru(TPA)(diimine)(solvent)]^{2+}$, which contains a facially tridentate TPA ligand and a less hindered solvent molecule with π-acceptor character. This thermal process completely and irreversibly proceeds via an associative transition state by an I_a mechanism. The starting materials and dissociation products undergo photochemical structural change reversibly to reach the photostationary states, which demonstrates the bistability of the two components. The photochemical process is proposed to proceed by a dissociative mechanism involving a five-coordinate intermediate with a vacant site. The quantum yields of forward and backward reactions could be determined to evaluate the efficiency of the photochemical structural change from both sides. This is the first example of isolation of the photoproduct and evaluation of the photochemical reactions of metal complexes from both the starting complexes and the photoproducts involving intermolecular reactions. Since the photochemical conversion is governed by the quantum yields and absorption coefficients, the amounts of components in the photostationary states can be regulated by means of the photoirradiation wavelength. Thus, we could achieved about 90% reversible regulation of the structural change by taking advantage of the complete thermal process and well-controlled photochemical process, as shown in Scheme 4. The process allows us to achieve acceptance and release of a guest molecule by molecular recognition in terms of its electronic character and bulkiness. Our systems on the basis of transition metal complexes could provide a new strategy to construct novel photofunctional molecular devices.

Experimental Section

Materials: Methanol in extra-pure grade was used without further purification. Diimine ligands were purchased from commercial sources and used without further purification. $[\{RuCl(TPA\ derivative)\}_2](ClO_4)_2$ were synthesized as reported previously[20] and their PF_6^- salts were prepared by ion exchange by adding an excess of nBu_4NPF_6 in methanol. *N*-(5-Methyl-2-pyridylmethyl)-*N*,*N*-bis(2-pyridylmethyl)amine (5-Me-TPA) was synthesized by reaction of 5-methyl-2-chloromethylpyridine with bis(2-pyridylmethyl)amine in CH_2Cl_2 in the presence of NEt_3. 5-Me_3-TPA·3 $HClO_4$ was synthesized as reported.[35]

$[Ru(TPA)(bpy)](PF_6)_2$ (1): Solid $[RuCl(TPA)]_2(ClO_4)_2$ (0.15 g, 0.14 mmol) was added to a degassed solution of bpy (0.15 g, 0.96 mmol) in MeOH (20 mL) under N_2. The mixture was heated to reflux for 8 h and then cooled to room temperature. NH_4PF_6 (91 mg, 0.56 mmol) was added to the solution to give an orange precipitate, which was washed well with diethyl ether and then dried in vacuo. Yield: 73%. Elemental analysis (%) calcd for $C_{28}H_{26}N_6P_2F_{12}Ru$: C 40.13, H 3.13, N 10.03; found: C 40.16, H 3.16, N 10.09; ^1H NMR (CD_3CN): $\delta = 9.56$ (d, 1H, $J = 6$ Hz; bpy-H6(equatorial)), 9.03 (d, 1H, $J = 6$ Hz; bpy-H6(axial)), 9.00 (d, 1H, $J = 6$ Hz; pyr-H6(axial)), 8.49 (d, 1H, $J = 8$ Hz; bpy-H3(equatorial)), 8.38 (d, 1H, $J = 8$ Hz; pyr-H3(axial)), 8.21 (td, 1H, $J = 7$, 1 Hz; bpy-H4(equatorial)), 7.94 (t, 1H, $J = 6$ Hz; bpy-H5(equatorial)), 7.91 (t, 1H, $J = 7$ Hz; pyr-H4(axial)), 7.68 (t, 2H, $J = 7$ Hz; pyr-H4(equatorial)), 7.66 (d, 2H, $J = 6$ Hz; pyr-H6(equatorial)), 7.63 (td, 2H, $J = 7$, 1 Hz; py-H4(equatorial)), 7.47 (td, 1H, $J = 7$ Hz, 1 Hz; pyr-H5(axial)), 7.38 (d, 1H, $J = 8$ Hz; bpy-H3(axial)), 7.34 (d, 2H, $J = 8$; pyr-H3(equatorial)), 7.27 (t, 1H, $J = 7$ Hz; bpy-H5(axial)), 6.99 (t, 2H, $J = 7$ Hz; pyr-H5(equatorial)), 5.43 and 5.07 (ABq, 4H, $J_{AB} = 18$ Hz; CH_2(equatorial)), 4.66 ppm (s, 2H; CH_2(axial)); ESIMS: m/z: 693.2 $[M^+]$; absorption maximum: $\lambda_{max} = 453$ nm.

$[Ru(TPA)(bpm)](PF_6)_2$ (2): Solid $[RuCl(TPA)]_2(ClO_4)_2$ (0.15 g, 0.14 mmol) was added to a degassed solution of bpm (0.15 g, 0.96 mmol) in MeOH (20 mL) under N_2. The mixture was heated to reflux for 8 h and then cooled to room temperature. NH_4PF_6 (91 mg, 0.56 mmol) was added to the solution to give a brown precipitate, which was washed well with diethyl ether and then dried in vacuo. Yield: 69%. Elemental analysis (%) calcd for $C_{26}H_{24}N_8P_2F_{12}Ru{\cdot}H_2O$: C 36.35, H 2.77, N 13.03; found: C 36.41, H 2.82, N 13.07; ^1H NMR (CD_3CN): $\delta = 9.88$ (dd, 1H, $J = 5$ Hz, 1 Hz; bpm-H6(equatorial)), 9.26 (d, 1H, $J = 4$ Hz; bpm-H6(axial)), 9.25 (d, 1H, $J = 5$ Hz; bpm-H4(equatorial)), 8.97 (d, 1H, $J = 5$ Hz; pyr-H6-(axial)), 8.93 (dd, 1H, $J = 5$, 1 Hz; bpm-H4(axial)), 8.03 (t, 1H, $J = 5$ Hz; bpm-H5(equatorial)), 7.77 (d, 2H, $J = 5$ Hz; pyr-H6(equatorial)), 7.70 (t, 1H, $J = 8$ Hz; pyr-H4(axial)), 7.64 (t, 2H, $J = 7$ Hz; pyr-H4(equatorial)), 7.58 (t, 1H, $J = 6$ Hz; bpm-H5(axial)), 7.38 (d, 2H, $J = 8$ Hz; pyr-H3(equatorial)), 7.35 (d, 1H, $J = 5$ Hz; pyr-H3(axial)), 7.30 (t, 1H, $J = 6$ Hz; pyr-H5(axial)), 7.03 (t, 2H, $J = 6$ Hz; pyr-H5(equatorial)), 5.35 and 5.11 (ABq, $J_{AB} = 17$, 4H; CH_2(equatorial)), 4.70 ppm (s, 2H, CH_2(axial)); ESIMS: m/z: 695.1 $[M^+]$; absorption maximum: $\lambda_{max} = 480$ nm.

$[Ru(TPA)(phen)](PF_6)_2$ (3): Solid $[RuCl(TPA)]_2(ClO_4)_2$ (0.15 g, 0.14 mmol) was added to a degassed solution of phen (0.15 g, 0.83 mmol) in MeOH (20 mL) under N_2. The mixture was heated to reflux for 8 h and then cooled to room temperature. NH_4PF_6 (91 mg, 0.56 mmol) was added to the solution to give an orange precipitate, which was washed well with diethyl ether and then dried in vacuo. Yield: 75%. Elemental analysis (%) calcd for $C_{30}H_{26}N_6P_2F_{12}Ru$: C 41.82, H 3.04, N 9.75; found:

 © 2008 Wiley-VCH Verlag GmbH & Co. KGaA, Weinheim

C 41.80, H 3.13, N 9.74; ^{1}H NMR (CD_3CN): $\delta = 9.98$ (d, 1H, $J = 5$ Hz; phen-H2), 9.40 (d, 1H, $J = 6$ Hz; phen-H9), 9.22 (d, 1H, $J = 6$ Hz; pyr-H6(axial)), 8.77 (d, 1H, $J = 8$ Hz; phen-H4), 8.49 (d, 1H, $J = 8$ Hz; phen-H7), 8.28 (q, 1H, $J = 6$ Hz; phen-H3), 8.26 (d, 2H, $J = 6$ Hz; phen-H5), 8.14 (d, 1H, $J = 9$ Hz; phen-H6), 7.81 (q, 1H, $J = 5$ Hz; phen-H8), 7.71 (td, 1H, $J = 8$, 1 Hz; pyr-H4(axial)), 7.57 (t, 2H, $J = 5$ Hz; pyr-H4(equatorial)), 7.55 (d, 2H, $J = 4$ Hz; pyr-H6(equatorial)), 7.39 (d, 1H, $J = 8$ Hz; pyr-H3(axial)), 7.36 (d, 2H, $J = 4$ Hz; pyr-H3(equatorial)), 7.33 (t, 1H, $J = 5$ Hz; pyr-H5(axial)), 6.85 (t, 2H, $J = 7$ Hz; pyr-H5(equatorial)), 5.57 and 5.16 (ABq, $J_{AB} = 17$, 4H; CH_2(equatorial)), 4.74 ppm (s, 2H, CH_2-(axial)); ESIMS: m/z: 717.1 [M^+]; absorption maximum: $\lambda_{max} = 423$ nm.

[Ru(TPA)(bpy)(CH_3CN)](PF_6)$_2$ (4): A solution of [Ru(TPA)(bpy)](PF_6)$_2$ (50 mg) in CH_3CN (100 mL) was heated to reflux for 24 h and evaporated to dryness to obtain a light orange powder. The powder was washed with diethyl ether and then dried in vacuo. Elemental analysis (%) calcd for $C_{30}H_{29}N_7P_2F_{12}Ru$: C 41.01, H 3.33, N 11.16; found: C 40.73, H 3.31, N 11.14; ^{1}H NMR (CD_3CN): $\delta = 8.92$ (d, 2H, $J = 6$ Hz; bpy-H2), 8.52 (d, 2H, $J = 8$ Hz; pyr-H6(equatorial)), 8.52 (d, 1H, $J = 8$ Hz; pyr-H6(free)), 8.34 (d, 2H, $J = 5$ Hz; pyr-H3(equatorial)), 8.13 (td, 2H, $J = 8$, 2 Hz; pyr-H5(equatorial)), 7.80 (td, 2H, $J = 8$, 1 Hz; bpy-H4), 7.70 (td, 1H, $J = 8$, 2 Hz; pyr-H4(free)), 7.56 (td, 2H, $J = 7$, 1 Hz; pyr-H4(equatorial)), 7.37 (d, 1H, $J = 8$ Hz; pyr-H5(free)), 7.35 (d, 2H, $J = 8$ Hz; bpy-H5), 7.34 (t, 2H, $J = 6$ Hz; bpy-H3), 7.09 (d, 1H, $J = 8$ Hz; pyr-H3(free)), 4.65 and 4.15 (ABq, 4H, $J_{AB} = 17$ Hz; CH_2(equatorial)), 3.22 (s, 2H, CH_2(free)), 2.27 ppm (s, 3H; CH_3); ESIMS: m/z: 734.2 [M^+]; absorption maximum: $\lambda_{max} = 426$ nm.

[Ru(TPA)(bpm)(CH_3CN)](PF_6)$_2$ (5): A solution of [Ru(TPA)(bpm)]-(PF_6)$_2$ (50 mg) in CH_3CN (100 mL) was heated to reflux for 24 h and evaporated to dryness to obtain a brownish orange powder. The powder was washed with diethyl ether and then dried in vacuo. Elemental analysis (%) calcd for $C_{28}H_{27}N_7P_2F_{12}Ru$: C 38.19, H 3.09, N 14.32; found: C 37.87, H 3.09, N 14.08; ^{1}H NMR (CD_3CN): $\delta = 9.16$ (dd, 2H, $J = 5$, 2 Hz; bpm-H6), 8.89 (d, 2H, $J = 7$ Hz; pyr-H6(equatorial)), 8.51 (dd, 2H, $J = 6$, 2 Hz; bpm-H4), 8.49 (d, 1H, $J = 4$ Hz; pyr-H6(free)), 7.85 (td, 2H, $J = 7$, 1 Hz; pyr-H4(equatorial)), 7.69 (t, 1H, $J = 6$ Hz; pyr-H4(free)), 7.65 (t, 2H, $J = 5$ Hz; bpm-H5), 7.41 (t, 2H, $J = 8$ Hz; pyr-H5(equatorial)), 7.41 (t, 2H, $J = 8$ Hz; pyr-H3(equatorial)), 7.33 (t, 1H, $J = 7$ Hz; pyr-H5(free)), 7.08 (d, 1H, $J = 8$ Hz; pyr-H3(free)), 4.74 and 4.24 (ABq, $J_{AB} = 17$ Hz, 4H; CH_2(equatorial)), 3.48 (s, 2H, CH_2(axial)), 2.27 ppm (s, 3H; CH_3); ESIMS: m/z: 736.2 [M^+]; absorption maximum: $\lambda_{max} = 453$ nm.

[Ru(TPA)(phen)(CH_3CN)](PF_6)$_2$ (6): A solution of [Ru(TPA)(phen)]-(PF_6)$_2$ (50 mg) in CH_3CN (100 mL) was heated to reflux for 24 h and evaporated to dryness to obtain a light orange powder. The powder was washed with diethyl ether and then dried in vacuo. Elemental analysis (%) calcd for $C_{32}H_{29}N_7P_2F_{12}Ru$: C 42.58, H 3.23, N 10.86; found: C 42.38, H 3.27, N 10.83; ^{1}H NMR (CD_3CN): $\delta = 9.00$ (d, 2H, $J = 5$ Hz; phen-H2), 8.68 (d, 2H, $J = 7$ Hz; pyr-H6(equatorial)), 8.60 (d, 2H, $J = 5$ Hz; pyr-H3(equatorial)), 8.40 (d, 1H, $J = 5$ Hz; pyr-H6(free)), 8.24 (s, 2H; phen-H5), 7.88 (t, 2H, $J = 6$ Hz; pyr-H5(equatorial)), 7.83 (t, 2H, $J = 8$ Hz; phen-H4), 7.55 (t, 1H, $J = 8$ Hz; pyr-H4(free)), 7.44 (t, 2H, $J = 6$ Hz; pyr-H4(equatorial)), 7.42 (t, 2H, $J = 4$ Hz; phen-H3), 7.21 (t, 1H, $J = 7$ Hz; pyr-H5(free)), 6.82 (d, 1H, $J = 8$ Hz; pyr-H3(free)), 4.77 and 4.18 (ABq, $J_{AB} = 17$ Hz, 4H; CH_2(equatorial)), 3.09 (s, 2H, CH_2(free)), 2.15 ppm (s, 3H; CH_3); ESIMS: m/z: 758.2 [M^+]; absorption maximum: $\lambda_{max} = 423$ nm.

[RuCl(TPA)(bpy)]PF_6 (7): Solid [(C_2H_5)$_4$N]Cl (0.28 g, 1.7 mmol) was added to a degassed solution of [Ru(TPA)(bpy)(CH_3CN)](PF_6)$_2$ (30 mg, 0.034 mmol) in CH_3CN (30 mL). The mixture was heated to reflux for 24 h, and the color of the solution changed from orange to dark purple. After removing the solvent by rotary evaporator, a small volume of water was added, and insoluble materials were filtered off to obtain a purple solution. A purple powder of **7** was obtained by removing the solvent. The powder was washed with a small amount of water and then dissolved in acetone. Hexane was added onto the acetone solution to form a two-layered system. Dark purple crystals of **7** formed. Elemental analysis (%) calcd for $C_{28}H_{26}N_6ClPF_6Ru$: C 45.63, H 3.69, N 11.40; found: C 45.69, H 3.83, N 11.14; ^{1}H NMR (CD_3CN): $\delta = 9.48$ (d, 2H, $J = 6$ Hz; bpy-H2), 8.51 (d, 1H, $J = 5$ Hz; pyr-H6(free)), 8.49 (d, 2H, $J = 7$ Hz; pyr-H6(equatorial)), 8.44 (d, 2H, $J = 7$ Hz; pyr-H3(equatorial)), 7.94 (td, 2H, $J = 7$, 1 Hz; pyr-H5(equatorial)), 7.69 (td, 2H, $J = 8$, 1 Hz; bpy-H4), 7.66 (td, 1H, $J = 8$, 1 Hz; pyr-H4(free)), 7.43 (td, 2H, $J = 8$, 1 Hz; pyr-H4(equatorial)), 7.32 (d, 2H, $J = 6$ Hz; bpy-H3), 7.30 (t, 2H, $J = 7$ Hz; pyr-H5(free)), 7.29 (d, 2H, $J = 8$ Hz; bpy-H5), 7.05 (d, 1H, $J = 8$ Hz; pyr-H3(free)), 4.50 and 3.98 (ABq, $J_{AB} = 16$ Hz, 4H; CH_2(equatorial)), 3.20 ppm (s, 2H; CH_2(free)); ESIMS: m/z: 583.3 [M^+]; absorption maximum: $\lambda_{max} = 503$ nm.

[RuCl(TPA)(bpm)]PF_6 (8): Solid [(C_2H_5)$_4$N]Cl (0.28 g, 1.7 mmol) was added to a degassed solution of [Ru(TPA)(bpm)(CH_3CN)](PF_6)$_2$ (30 mg, 0.034 mmol) in CH_3CN (30 mL). The mixture was heated to reflux for 24 h, and the color of the solution changed from orange to dark purple. After removing the solvent by rotary evaporator, a small volume of water was added and insoluble materials were filtered off to obtain a purple solution. A purple powder of **8** was obtained by removing the solvent. Elemental analysis (%) calcd for $C_{26}H_{24}N_8ClPF_6Ru$: C 42.78, H 3.31, N 15.35; found: C 42.66, H 3.35, N 15.17; ^{1}H NMR (CD_3CN): $\delta = 9.41$ (d, 2H, $J = 6$ Hz; pyr-H6(equatorial)), 8.98 (dd, 2H, $J = 7$, 2 Hz; bpm-H6), 8.57 (dd, 2H, $J = 7$, 2 Hz; bpm-H4), 8.47 (d, 1H, $J = 4$ Hz; pyr-H6(free)), 7.76 (td, 2H, $J = 7$, 2 Hz; pyr-H4(equatorial)), 7.65 (td, 1H, $J = 7$, 2 Hz; pyr-H4(free)), 7.51 (t, 2H, $J = 5$ Hz; bpm-H5), 7.35 (t, 2H, $J = 7$ Hz; pyr-H5(equatorial)), 7.35 (t, 1H, $J = 7$ Hz; pyr-H3(equatorial)), 7.28 (t, 1H, $J = 7$ Hz; pyr-H5(free)), 7.03 (d, 1H, $J = 8$ Hz; pyr-H3(free)), 4.66 and 4.11 (ABq, $J_{AB} = 17$ Hz, 4H; CH_2(equatorial)), 3.52 ppm (s, 2H; CH_2(axial)); ESIMS: m/z: 585.1 [M^+]; absorption maximum: $\lambda_{max} = 539$ nm.

[RuCl(TPA)(phen)]PF_6 (9): Solid [(C_2H_5)$_4$N]Cl (0.28 g, 1.7 mmol) was added to a degassed solution of [Ru(TPA)(phen)(CH_3CN)](PF_6)$_2$ (30 mg, 0.033 mmol) in CH_3CN (30 mL). The mixture was heated to reflux for 24 h, and the color of the solution changed from orange to dark purple. After removing the solvent by rotary evaporator, a small volume of water was added and insoluble materials were filtered off to obtain a brown solution. A brown powder of **9** was obtained by removing the solvent. Elemental analysis (%) calcd for $C_{30}H_{26}N_6ClPF_6Ru\cdot 0.5H_2O$: C 47.91, H 3.48, N 11.17; found: C 47.74, H 4.03, N 10.92; ^{1}H NMR (CD_3CN): $\delta = 9.56$ (d, 2H, $J = 6$ Hz; phen-H2), 8.67 (d, 2H, $J = 7$ Hz; pyr-H6(equatorial)), 8.47 (d, 2H, $J = 7$ Hz; pyr-H3(equatorial)), 8.37 (d, 1H, $J = 7$ Hz; pyr-H6(free)), 8.16 (s, 2H; phen-H5), 7.78 (td, 2H, $J = 8$, 1 Hz; pyr-H5(equatorial)), 7.76 (td, 2H, $J = 8$, 1 Hz; phen-H4), 7.50 (t, 1H, $J = 8$ Hz; pyr-H4(free)), 7.38 (t, 2H, $J = 6$ Hz; pyr-H4(equatorial)), 7.36 (t, 2H, $J = 7$ Hz; phen-H3), 7.18 (td, 1H, $J = 7$, 1 Hz; pyr-H5(free)), 6.77 (d, 1H, $J = 8$ Hz; pyr-H3(free)), 4.64 and 4.03 (ABq, $J_{AB} = 18$ Hz, 4H; CH_2(equatorial)), 3.11 ppm (s, 2H; CH_2(free)); ESIMS: m/z: 607.3 [M^+]; absorption maximum: $\lambda_{max} = 495$ nm.

[Ru(5-Me_3-TPA)(bpy)](PF_6)$_2$ (10): Solid [RuCl(5-Me_3TPA)]$_2$(ClO_4)$_2$ (50 mg, 0.057 mmol) was added to a degassed solution of bpy (36 mg, 0.23 mmol) in MeOH (20 mL)under N_2. The mixture was heated to reflux for 8 h and then cooled to room temperature. NH_4PF_6 (18 mg, 0.11 mmol) was added to the solution to give an orange precipitate, which was washed well with diethyl ether and then dried in vacuo. Yield: 73%. Elemental analysis (%) calcd for $C_{31}H_{32}N_6P_2F_{12}Ru$: C 42.33, H 3.67, N 9.55; found: C 42.53, H 3.68, N 9.57; ^{1}H NMR (CD_3CN): $\delta = 9.58$ (d, 1H, $J = 5$ Hz; bpy-H6(equatorial)), 8.99 (d, 1H, $J = 6$ Hz; bpy-H6-(axial)), 8.85 (s, 1H; pyr-H6(axial)), 8.49 (d, 1H, $J = 8$ Hz; bpy-H3(equatorial)), 8.38 (d, 1H, $J = 8$ Hz; bpy-H3(axial)), 8.21 (t, 1H, $J = 7$ Hz; bpy-H4(equatorial)), 7.97 (t, 1H, $J = 6$ Hz; bpy-H5(equatorial)), 7.92 (t, 1H, $J = 7$ Hz; bpy-H4(axial)), 7.48 (s, 2H; pyr-H6(equatorial)), 7.47 (d, 1H, $J = 7$ Hz; pyr-H3(axial)), 7.44 (t, 1H, $J = 7$ Hz; bpy-H5(axial)), 7.41 (d, 2H, $J = 6$; pyr-H3(equatorial)), 7.23 (d, 1H, $J = 5$ Hz; pyr-H4(axial)), 7.20 (d, 2H, $J = 6$ Hz; pyr-H4(equatorial)), 5.37 and 4.99 (ABq, 4H, $J_{AB} = 17$ Hz; CH_2(equatorial)), 4.57 (s, 2H; CH_2(axial)), 2.28 (s, 3H; CH_3-(axial)), 1.97 ppm (s, 6H, CH_3(equatorial)); ESIMS: m/z: 735.3 [$M-PF_6^-$]$^+$; absorption maximum: $\lambda_{max} = 453$ nm.

[Ru(5-Me_3-TPA)(bpy)(CD_3CN)](PF_6)$_2$ (11): A solution of [Ru(5-Me_3-TPA)(bpy)](PF_6)$_2$ in CD_3CN (0.6 mL) was heated at 70 °C for 30 h in an NMR sample tube. ^{1}H NMR (CD_3CN): $\delta = 8.72$ (s, 2H; pyr-H4(equatorial)), 8.50 (d, 2H, $J = 8$ Hz; bpy-H6), 8.29 (s, 1H; pyr-H6(free)), 8.28 (d, 2H, $J = 6$ Hz; bpy-H3), 8.11 (td, 2H, $J = 8$, 2 Hz; bpy-H5), 7.61 (d, 2H,

 © 2008 Wiley-VCH Verlag GmbH & Co. KGaA, Weinheim

$J=7$ Hz; pyr-H3(equatorial)), 7.54 (td, 1H, $J=6$, 2 Hz; bpy-H4), 7.49 (d, 1H, $J=6$ Hz; pyr-H3(free)), 7.21 (d, 2H, $J=8$ Hz; pyr-H4(equatorial)), 6.94 (d, 1H, $J=8$ Hz; pyr-H4(free)), 4.87 and 3.75 (ABq, 4H, $J_{AB}=17$ Hz; CH_2(equatorial)), 3.15 (s, 2H, CH_2(axial)), 2.36 (s, 6H; CH_3(equatorial)), 2.29 ppm (s, 3H; CH_3(axial)); ESIMS: m/z: 778.7 [M^+].

[Ru(5-Me-TPA)(bpy)](PF$_6$)$_2$ (12): NaOH (2.0 equiv) and solid $RuCl_3\cdot 3H_2O$ (260 mg, 1.00 mmol) were added to a degassed solution of *N*,*N*-bis(2-pyridinylmethyl)-*N*-(5-methyl-2-pyridylmethyl)amine triperchlorate (5-Me-TPA·3HClO$_4$, 266 mg, 1.00 mmol) in EtOH (75 mL) under N_2. The mixture was heated to reflux for 12 h and then filtered to obtain a brownish orange solid. Solid bpy (112 mg, 0.72 mmol) was added to a degassed solution of the powder (100 mg) in MeOH (20 mL) under N_2. The mixture was heated to reflux for 8 h and then cooled to room temperature. NH_4PF_6 (91 mg, 0.56 mmol) was added to the solution to obtain an orange precipitate, which was washed well with diethyl ether and then dried in vacuo. Yield: 32% (as a mixture of isomers). Elemental analysis (%) calcd for $C_{29}H_{28}N_6P_2F_{12}Ru$: C 40.90, H 3.31, N 9.86; found: C 41.10, H 3.47, N 9.87; ^{1}H NMR (CD_3CN): $\delta=2.27$ (s, 3H; CH_3(axial)), 1.97 ppm (s, 6H; CH_3(equatorial)); ESIMS: 707.2 [M^+].

[Ru(5-Me-TPA)(bpy)(CD$_3$CN)](PF$_6$)$_2$ (13): A solution of [Ru(5-Me-TPA)(bpy)](PF$_6$)$_2$ in CD_3CN (0.6 mL) was heated at 70°C for 30 h in an NMR tube; ^{1}H NMR (CD_3CN): $\delta=2.35$ (s, 6H; CH_3(equatorial)), 2.29 ppm (s, 3H; CH_3(axial)); ESIMS: m/z: 751.2 [M^+].

X-ray crystallography: **1**: A single crystal of **1** suitable for X-ray analysis was obtained by recrystallization of its PF_6^- salt. The crystal was mounted on a glass capillary with epoxy resin. Diffraction data were collected on a Rigaku R-AXIS RAPID Imaging Plate diffractometer with graphite-monochromated $Mo_{K\alpha}$ radiation ($\lambda=0.7107$ Å) at 23°C. Using ω scans of 44 exposures with 5.0° step at 3 min per degree up to $2\theta_{max}=54.7°$, a total of 26599 reflections were collected and then merged to provide unique 7310 data ($R_{int}=0.049$), of which 7304 (all data) were used to solve the structure. The structure was solved by direct methods (SIR 92) and refined by full-matrix least-squares methods on F^2. All non-hydrogen atoms were refined anisotropically. All calculations were done with the teXsan program package.[36] The final differential Fourier map showed a maximum peak of 0.95 e Å^{-3} and a minimum of −0.68 e Å^{-3}. Crystallographic data for **1** are summarized in Table 6.

2 and 3: Single crystals of **2** and **3** were obtained by recrystallization of crude product from methanol. The crystals were mounted on a glass capillary with silicon grease and diffraction data were collected on a Rigaku Mercury CCD diffractometer with a rotating anode X-ray tube at −150°C with graphite-monochromated $Mo_{K\alpha}$ radiation ($\lambda=0.7107$ Å). The structure was solved by direct methods (SIR 97) and refined by full-matrix least-squares methods on F^2 by using the CrystalStructure program package.[37] The final differential Fourier map for **2** showed a maximum peak of 4.57 e Å^{-3} near a severely disordered PF_6^- ion and a minimum of −1.95 e Å^{-3}. For **3**, the final Fourier map exhibited a maximum peak of 1.63 e Å^{-3} and a minimum peak of −0.89 e Å^{-3}. Crystallographic data for **2** and **3** are summarized in Table 6.

[RuCl(TPA)(bpy)]PF$_6$·(CH$_3$)$_2$CO (7·(CH$_3$)$_2$CO) and [RuCl(TPA)-(bpm)]PF$_6$ (8): Single crystals were obtained by recrystallization of the crude product from acetone by vapor diffusion of diethyl ether for **7**,[38] and from acetone by vapor diffusion of hexanes for **8**. The crystals were mounted on a glass capillary with silicon grease, and diffraction data were collected on a Rigaku Mercury CCD diffractometer with a rotating-anode X-ray tube at −150°C with graphite-monochromated $Mo_{K\alpha}$ radiation ($\lambda=0.7107$ Å). The structure was solved by direct methods (SIR 97) and refined by full-matrix least-squares methods on F^2 by using the CrystalStructure program package.[37] All non-hydrogen atoms were refined anisotropically. The final Fourier map exhibited a maximum peak of 1.36 e Å^{-3} and a minimum peak of −1.62 e Å^{-3} for **7·(CH$_3$)$_2$CO**, and 0.82 and −0.72 e Å^{-3}, respectively, for **8**. Crystallographic data for **7·(CH$_3$)$_2$CO** and **8** are summarized in Table 6.

CCDC 686782 (**2**), 686783 (**3**), 686785 (**7**) and 686784 (**8**) contain the supplementary crystallographic data for this paper. These data can be obtained free of charge from The Cambridge Crystallographic Data Centre via www.ccdc.cam.ac.uk/data_request/cif.

Spectroscopic measurements: Absorption spectra were measured on Jasco V-570 and Shimadzu UV-3100 spectrophotometers in CH_3CN at room temperature. ^{1}H NMR spectra were obtained on JEOL EX-270 and AL-300 spectrometers, and chemical shifts were determined by using the residual solvent peak as a reference. ESIMS spectra were recorded on a Perkin-Elmer API-150 spectrometer.

Photochemical reactions: Photoirradiation of the samples was performed by using the light source of a Shimadzu RF-5300PC fluorescence spectrophotometer at monochromated wavelengths (423, 453, and 480 nm) in CH_3CN at room temperature. The reaction was done in an NMR tube or a 10 mm quartz cell to monitor the progress of the reaction by NMR and absorption spectroscopy, respectively.

Quantum yield determination: Quantum yields of the forward and backward reactions were determined by a standard method using an actinometer (potassium ferrioxalate) in CH_3CN at room temperature with photoirradiation at 423 nm. Absorptions of the complexes and the actinometer were uniformed at 423 nm to determine the quantum yields. The reactions were monitored at appropriate wavelengths to observe the time

Table 6. X-ray crystallographic data for **1**–**3**, **7**, and **8**.

	1	**2**	**3**	**7**	**8**
formula	$C_{28}H_{26}N_6F_{12}P_2Ru$	$C_{26}H_{24}N_8F_{12}P_2Ru$	$C_{30}H_{32}N_6O_3F_{12}P_2Ru$	$C_{31}H_{32}N_6OClF_6PRu$	$C_{26}H_{24}N_8ClF_6PRu$
FW	837.55	839.53	915.62	786.1	730.0
crystal system	monoclinic	triclinic	monoclinic	orthorhombic	monoclinic
space group	$P2_1/n$	$P\bar{1}$	$P2_1/n$	$Pnma$	$P2_1/n$
T [K]	296	123	123	123	123
a [Å]	13.0220(9)	11.487(4)	12.406(2)	18.82(1)	14.186(14)
b [Å]	18.463(1)	12.284(1)	20.150(4)	23.64(1)	10.288(12)
c [Å]	13.8049(9)	13.424(1)	13.927(3)	15.473(8)	19.679(18)
α [°]		73.48(7)			
β [°]	101.116(1)	69.63(7)	97.772(2)		102.62(2)
γ [°]		63.09(6)			
V [Å^3]	3256.8(4)	1565.2(8)	3449.4(1)	6883(6)	2803(5)
Z	4	2	4	8	4
no. of reflns	26599	11332	26677	45523	21048
no. of obsd reflns	7310	6342	7841	8072	6383
no. of parameters	442	443	488	441	389
$R1$[a] [$I>2.0\sigma(I)$]	0.050	0.050	0.052	0.130	0.035
$wR2$[b] (all data)	0.128	0.128	0.151	0.329	0.077
GOF	1.09	1.05	1.13	1.06	1.04

[a][a] $R_1=\Sigma||F_o|-|F_c||/\Sigma|F_o|$. [b] $wR_2=[\Sigma w(F_o^2-F_c^2)^2/\Sigma w(F_o^2)^2]^{1/2}$.

© 2008 Wiley-VCH Verlag GmbH & Co. KGaA, Weinheim

course of the increase or decrease of the absorptions, and the data in the initial stage during which the time course exhibited linear change was used to determine the quantum yields.

Acknowledgements

We thank Prof. Kenji Matsuda (Kyushu University) for his invaluable advice. This work was partially supported by a Grant-in-Aid (No. 19205019) from The Ministry of Education, Culture, Sports, Science and Technology of Japan.

[1] V. Balzani, M. Venturi, A. Credi, *Molecular Devices and Machines—A Journey to the Nanoworld*, Wiley-VCH, Weinheim, **2003**.
[2] B. Alberts, D. Bray, J. Lewis, M. Raff, K. Roberts, J. D. Watson, *Molecular Biology of the Cell*, 3rd ed., Garland Publishing, New York, **1994**, p. 46.
[3] H. Itoh, A. Takahashi, K. Adachi, H. Noji, R. Yasuda, M. Yoshida, K. Kinoshita, Jr., *Nature* **2004**, *427*, 465–468.
[4] O. P. Ernst, F. J. Bartl, *ChemBioChem* **2002**, *3*, 968–974, and references therein.
[5] a) J. Vicario, M. Walko, A. Meetsma, B. L. Ferringa, *J. Am. Chem. Soc.* **2006**, *128*, 5127–5135; b) N. Koumura, R. W. Zijlstra, R. A. van Delden, N. Harada, B. L. Ferringa, *Nature* **1999**, *401*, 152; c) T. Shimasaki, S. Kato, K. Ideta, K. Goto, T. Shinmyozu, *J. Org. Chem.* **2007**, *72*, 1073–1087; d) T. Muraoka, K. Kinbara, T. Aida, *Nature* **2006**, *440*, 512–515; e) S. Saha, J. F. Stoddart, *Chem. Soc. Rev.* **2007**, *36*, 77–92.
[6] T. Arai, K. Tokumaru, *Chem. Rev.* **1993**, *93*, 23–39.
[7] J. D. Badjic, V. Balzani, A. Credi, S. Silvi, J. F. Stoddart, *Science* **2004**, *303*, 1845–1849.
[8] Redox-active heteroaromatic coenzymes such as pterins and flavins undergo planar–bent structural changes in the course of proton-coupled electron transfer: a) C.-C. Wei, B. R. Crane, D. J. Stuehr, *Chem. Rev.* **2003**, *103*, 2365–2383; b) D. J. Porter, D. Voet, *Acta Cryst. Sect. B* **1978**, *34*, 598–610.
[9] a) A. Petitjean, R. G. Khoury, N. Kyritsakas, J.-M. Lehn, *J. Am. Chem. Soc.* **2004**, *126*, 6637–6647; b) L. Jiang, J. Okano, A. Orita, J. Otera, *Angew. Chem.* **2004**, *116*, 2173–2176; *Angew. Chem. Int. Ed.* **2004**, *43*, 2121–2124.
[10] a) K. Matsuda, M. Irie, *Chem. Eur. J.* **2001**, *7*, 3466–3473; b) M. Irie, *Chem. Rev.* **2000**, *100*, 1685–1716.
[11] Y. Yokoyama, *Chem. Rev.* **2000**, *100*, 1717–1740, and references therein.
[12] C. Takayama, M. Kajitani, T. Sugiyama, T. Akiyama, K. Shimizu, A. Sugimori, *Organometallics* **1997**, *16*, 3498–3503.
[13] a) V. Aubert, V. Guerchais, E. Ishow, K. Hoang-Thi, I. Ledoux, K. Nakatani, H. Le Bozec, *Angew. Chem.* **2008**, *120*, 587–590; *Angew. Chem. Int. Ed.* **2008**, *47*, 577–580; b) K. Matsuda, K. Takayama, M. Irie, *Inorg. Chem.* **2004**, *43*, 482–489.
[14] a) S. Zahn, J. W. Canary, *Science* **2000**, *288*, 1404–1407; b) S. Zahn, J. W. Canary, *J. Am. Chem. Soc.* **2002**, *124*, 9204–9211; c) S. Zahn, D. Das, J. W. Canary, *Inorg. Chem.* **2006**, *45*, 6056–6063.
[15] a) C. A. Sassano, C. A. Mirkin, *J. Am. Chem. Soc.* **1995**, *117*, 11379–11380; b) E. T. Singewald, C. A. Mirkin, C. L. Stern, *Angew. Chem.* **1995**, *107*, 1725–1728; *Angew. Chem. Int. Ed. Engl.* **1995**, *34*, 1624–1627.
[16] a) D. Hesek, Y. Inoue, S. R. L. Everitt, *Chem. Lett.* **1999**, 109–110; b) H. Amouri, J. B. Waern, R. Caspar, A. Barbieri, C. Sabatini, A. Zanelli, F. Barigelletti, *Dalton Trans.* **2007**, 2179–2186; c) S. Bonnet, J.-P. Collin, N. Gruber, J.-P. Sauvage, E. R. Schofield, *Dalton Trans.* **2003**, 4654–4662; d) S. Bonnet, J.-P. Collin, J.-P. Sauvage, E. Schofield, *Inorg. Chem.* **2004**, *43*, 8346–8354.
[17] a) B. Durham, S. R. Wilson, D. J. Hodgson, T. J. Meyer, *J. Am. Chem. Soc.* **1980**, *102*, 600–607; b) See also: M. E. Rerek, P. S. Sheridan, *Inorg. Chem.* **1980**, *19*, 2646–2650.
[18] a) N. Armaroli, V. Balzani, J.-P. Collin, P. Gaviña, J.-P. Sauvage, B. Ventura, *J. Am. Chem. Soc.* **1999**, *121*, 4397–4408; b) P. Mobian, J.-M. Kern, J.-P. Sauvage, *Angew. Chem.* **2004**, *116*, 2446–2449; *Angew. Chem. Int. Ed.* **2004**, *43*, 2392–2395; c) E. Baranoff, F. Barigelletti, S. Bonnet, J.-P. Collin, L. Flamigni, P. Mobian, J.-P. Sauvage, *Struct. Bonding (Berlin)* **2007**, *123*, 41–78.
[19] T. Kojima, T. Sakamoto, Y. Matsuda, *Inorg. Chem.* **2004**, *43*, 2243–2245.
[20] a) T. Kojima, T. Amano, Y. Ishii, M. Ohba, Y. Okaue, Y. Matsuda, *Inorg. Chem.* **1998**, *37*, 4076–4085; b) T. Kojima, H. Matsuo, Y. Matsuda, *Inorg. Chim. Acta* **2000**, *300–302*, 661–667. **Safety note**: Perchlorate salts of metal complexes with organic ligands are potentially explosive. They should be handled with great care in small quantities.
[21] A. Guy Orpen, L. Brammer, F. H. Allen, O. Kennard, D. G. Watson, R. Taylor, *J. Chem. Soc. Dalton Trans.* **1989**, S1–S83.
[22] D. P. Rillema, G. Allen, T. J. Meyer, D. Conrad, *Inorg. Chem.* **1983**, *22*, 1617–1622.
[23] R. C. Young, T. J. Meyer, D. G. Whitten, *J. Am. Chem. Soc.* **1976**, *98*, 286–287.
[24] T. Kojima, K. Hayashi, Y. Shiota, Y. Tachi, Y. Naruta, T. Suzuki, K. Uezu, K. Yoshizawa, *Bull. Chem. Soc. Jpn.* **2005**, *78*, 2152–2158.
[25] T. Kojima, Y. Matsuda, *J. Chem. Soc. Dalton Trans.* **2001**, 958–960.
[26] In the preliminary communication,[19] we proposed a wrong structure for **4**, but we could clarify the structures of dissociation products in this study.
[27] a) R. W. Callahan, G. M. Brown, T. J. Meyer, *Inorg. Chem.* **1975**, *14*, 1443–1453; b) G. M. Bryant, J. E. Fergusson, H. K. J. Powell, *Aust. J. Chem.* **1971**, *24*, 257–273.
[28] S. Miyazaki, T. Kojima, S. Fukuzumi, *J. Am. Chem. Soc.* **2008**, *130*, 1556–1557.
[29] T. Kojima, S. Miyazaki, K. Hayashi, Y. Shimazaki, F. Tani, Y. Naruta, Y. Matsuda, *Chem. Eur. J.* **2004**, *10*, 6402–6410.
[30] J. E. Huheey, E. A. Keiter, R. L. Keiter, *Inorganic Chemistry*, 4th ed., HarperCollins College Publishers, New York, **1993**, pp. 540–543.
[31] K. Matsuda, M. Irie, *Chem. Eur. J.* **2001**, *7*, 3466–3473.
[32] A. Juris, V. Balzani, F. Barigelletti, S. Campagna, P. Belser, A. von Zelewsky, *Coord. Chem. Rev.* **1988**, *84*, 85–277.
[33] a) B. Durham, J. V. Casper, J. K. Nagle, T. J. Meyer, *J. Am. Chem. Soc.* **1982**, *104*, 4803–4810; b) C. R. Hecker, P. E. Fanwick, D. R. McMillin, *Inorg. Chem.* **1991**, *30*, 659–666; c) See also ref. [28].
[34] In the course of photoirradiation of a [D_6]DMSO solution of **1** at 453 nm, we observed formation of two photoproducts showing σ_h symmetry in the ^{1}H NMR spectrum (see Figure S6, Supporting Information). These two species exhibited one peak cluster in the ESIMS spectrum at *m*/*z* 777.1, assignable to {[Ru(bpy)([D_6]DMSO)(TPA)]PF_6}$^+$ [$M-PF_6^-$] (see Figure S7, Supporting Information). This may be derived from photoisomerization of the Ru-coordinated DMSO molecule between the S-bound and O-bound forms: a) M. K. Smith, J. A. Gibson, C. G. Young, J. A. Broomhead, P. C. Junk, F. R. Keene, *Eur. J. Inorg. Chem.* **2000**, 1365–1370; b) J. J. Rack, J. R. Winkler, H. B. Gray, *J. Am. Chem. Soc.* **2001**, *123*, 2432–2433; c) A. A. Rachford, J. J. Rack, *J. Am. Chem. Soc.* **2006**, *128*, 14318–14324.
[35] Y. Dong, H. Fujii, M. P. Hendrich, R. A. Leising, G. Pan, C. R. Randall, E. C. Wilkinson, Y. Zang, L. Que, Jr.; B. G. Fox, K. Kauffmann, E. Münck, *J. Am. Chem. Soc.* **1995**, *117*, 2778–2792; B. G. Fox, K. Kauffmann, E. Münck, *J. Am. Chem. Soc.* **1995**, *117*, 2778–2792.
[36] teXsan: Crystal Structure Analysis Package, Molecular Structure Corporation, **1985** and **1999**.
[37] CrystalStructure 3.7.0: Crystal Structure Analysis Package, Rigaku and Rigaku/MSC, The Woodlands, TX 77381, USA, **2000–2005**.
[38] In this case, the crystallographic analysis resulted in relatively high *R* values due to the poor quality of the crystal. However, the result is adequate to describe the geometry of **7**.

Received: May 1, 2008
Revised: June 14, 2008
Published online: August 19, 2008

 © 2008 Wiley-VCH Verlag GmbH & Co. KGaA, Weinheim